Supervisor: Jörgen Larsson

Investigation of thermal conductivity in thin graphite films through time-resolved X-ray diffraction

Thesis submitted for the degree
of Bachelor of Science

Project duration: 2 months

Abstract

Knowledge about thermal properties of nanoscale graphite is essential in order to realize the many promising applications of carbon based nanomaterials. This thesis reports how samples of thin graphite films on nickel substrates were investigated using time-resolved X-ray diffraction (TRXD) at the FemtoMAX beamline at the MAX IV facility. Through these investigations the thermal conductivity of the thin graphite films were determined by modeling the system using a one dimensional heat-diffusion model which was fitted to the data. Through investigation of the dynamics in the solid, it was determined that the thermal conductivity of graphite decreases with thinner graphite films as well as increased deposited energy.

Contents

1 Introduction

1.1 Motivation

Nanoscale carbon-based materials have interesting properties that make them suited for a large range of potential applications. In order to utilize these materials all these properties must be known. One interesting property of nanoscale graphite is the thermal conductivity which has been shown to be significantly lower than that of bulk graphite. [1]

It can be difficult to determine the properties because of the small dimensions of nanomaterials. However, there are techniques through which one can investigate these materials. One of the methods used to determine the properties of ultra-thin materials is time-resolved X-ray diffraction (TRXD).

TRXD is a powerful tool, which like most time-resolved experiments is conducted by utilizing the "pump-probe" method. This technique is comprised of first exciting the system using a pump pulse to cause a dynamic reaction. Then the system is investigated by using a probe pulse which measures the dynamical response. In the case of TRXD the probe pulse consists of X-rays, which are diffracted onto the sample. The resultant diffraction patterns carries information about the structure of the material such as the distance between the atomic planes. Since the technique is time-resolved it can be used to determine the dynamics of the structure.

In this project the thermal conductivity along the c-axis (orthogonally to the planes) of thin graphite films on nickel substrates was investigated using TRXD. The experiments were conducted at the FemtoMAX beamline at the MAX IV facility. The sample was heated by a laser pulse resulting in thermal expansion of the graphite film. Probing as the system returned to equilibrium provided information about the change in the interatomic distance between the graphite layers i.e. the changes in strain.

In order to determine the thermal conductivity, the system was modelled using a one-dimensional heat diffusion model, connecting the heat transport in the sample to the strain. The model was fitted to the experimental data in order to determine the value of the thermal conductivity.

Investigations such as these are important as they allow for better understanding of the properties of carbon nanomaterials. This is important for the understanding of how heat transfers in nanostructures and for the many possible applications. Such applications of nano-carbon includes improvements in solar cells, electrical components and medicine to mention a few.

1.2 Background

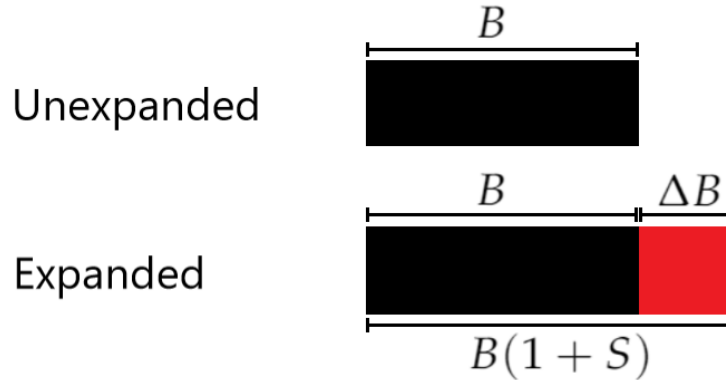### 1.2.1 Thermal expansion

Figure 1: Illustration of the different lengths in a comparison between expanded and unexpanded material.

The samples were heated with a laser resulting in thermal expansion. Thermal expansion is proportional to the temperature in the material and is calculated using equation eq. (1), ΔB, B, α, ΔT and S denotes the length of the expansion, original length of the material, the thermal expansion coefficient, temperature difference and the strain (the thermal expansion in fraction) respectively [3]. ΔB and B are illustrated in fig. 1.

$$\frac{\Delta B}{B} = \alpha \Delta T \iff S = \alpha \Delta T \tag{1}$$

The expanded interplanar distance is described in eq. (2), where d is the interplanar distance and d_0 is the unexcited interplanar distance.

$$d = d_0(1 + S) \tag{2}$$

Materials expand with the speed of sound in that material. This means that if one knows the expansion time one can calculate the thickness of a material as seen in eq. (3), b, t_{exp} and v_{sos} denote the material thickness, the expansion time and the speed of sound in the material respectively.

$$b = t_{exp}v_{sos} \tag{3}$$

1.2.2 Diffraction

The crystal structure of a graphite plane is that of a hexagonal (honeycomb like) arrangement. These planes are stacked on top of each other with a interplanar distance of d.

In order to measure the interplanar distance the system was probed using X-ray diffraction, which is described by Bragg's condition, given in eq. (4), θ, n and λ denotes the scattering angle (from the surface), interference order and wavelength of the incident X-rays respectively. If the condition is fulfilled it results in strong peaks called Bragg peaks. [2]

2

$$2d \sin \theta = n\lambda \tag{4}$$

The Bragg angle of interest is that of the (002) plane which is $27°$. As the system is thermally expanded, the interplanar distance is increased. Thus, the Bragg angle is changed in accordance with eq. (4). This shifts the position of the Bragg peaks.

1.2.3 Absorption of light

The absorption of light (e.g. from a laser) in matter is described by Beer–Lamberts law given in eq. (5), I, z, I_0 and δ denotes the intensity, the depth into the material, the intensity of the incident laser and the optical absorption depth of the material respectively. [4]

$$I(z) = I_0 \, exp\left(-\frac{z}{\delta}\right) \tag{5}$$

1.3 Modeling heat transfer
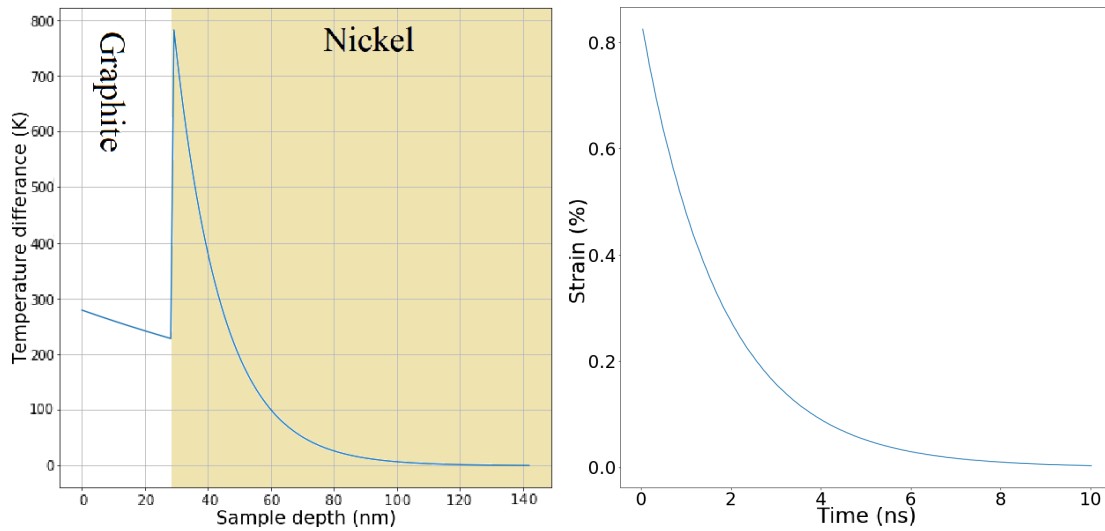
(a) initial heat distribution as temperature difference against depth into the sample. The different materials are labeled

(b) Strain as a function of time in the graphite film.

Figure 2: Images which illustrate different parts of the temperature model.

1.3.1 Temperature model

The system was modeled using a one dimensional heat diffusion equation [1] seen in eq. (6). In eq. (6), ρ, t and k denotes the the density, the time and the thermal conductivity respectively. The indexes denote whether the term concerns the graphite film or the nickel substrate.

$$\rho_i C_i \frac{\partial T}{\partial t} = \frac{\partial}{\partial z} k_i \frac{\partial T}{\partial z} \Leftrightarrow \frac{\partial T}{\partial t} = \frac{k_i}{\rho_i C_i} \frac{\partial^2 T}{\partial z^2} \tag{6}$$

3

The heat equation was rewritten in a numerical form as a Crank-Nicolson expression. The Crank-Nicolson formulation was chosen as it does not have any stability requirement [8]. This does not put any requirement on the step sizes in time or space allowing them to be set to reasonable values, which in turn allows one to complete the calculations with reasonable computational times. The Crank-Nicolson scheme for the heat diffusion equation in eq. (6) can be seen in eq. (7), a, h and NB_k are the step size in space, the step size in time and the number of adjacent Neumann boundaries, $\mathbf{A}$ and $\mathbf{B}$ are matrices containing the coefficients of the T variables which are combined into the $\mathbf{T}^{n+1}$ and $\mathbf{T}^n$ vectors. The scripts n and k denote the step in time and position respectively. The constants are combined as $r = \frac{h k_i}{a^2 \rho_i C_i}$.

$$
\begin{aligned}
\frac{T_k^{n+1} - T_k^n}{h} &= \frac{k_i}{\rho_i C_i} \frac{1}{2} \left(\frac{T_{k+1}^{n+1} + T_{k-1}^{n+1} - 2T_k^{n+1}}{a^2} + \frac{T_{k+1}^n + T_{k-1}^n - 2T_k^n}{a^2} \right) \\
&\Leftrightarrow (2 + 2r)T_k^{n+1} - rT_{k+1}^{n+1} - rT_{k-1}^{n+1} = (2 - 2r)T_k^n + rT_{k+1}^n + rT_{k-1}^n \\
&\hspace{4cm} \Leftrightarrow \mathbf{A}\mathbf{T}^{n+1} = \mathbf{B}\mathbf{T}^n
\end{aligned}
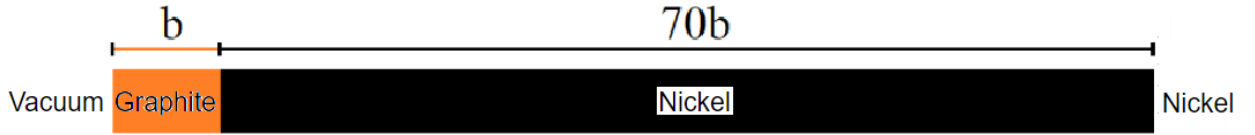\tag{7}
$$

1.3.2 Modeled system

Figure 3: Illustration of the modeled system (not to scale).

The system was modeled as a graphite film on a nickel substrate as seen in fig. 3. The model extended from the vacuum-graphite interface to 70 times the thickness of the graphite film into the nickel so that the heat had enough space to diffuse. The vacuum-graphite boundary was modeled as a Neumann boundary (a boundary over which the derivative is zero to ensure that no heat transfers over the boundary). This is because no significant heat should transfer from the material into the vacuum. The graphite-nickel and nickel-nickel boundaries were modeled to allow for temperature transfer. The temperature difference value for the nickel-nickel boundary was put to zero for all times

1.3.3 Initial heat profile

Using eq. (5) the initial temperature profile (the initial condition at time zero) in the sample after laser excitation can be calculated. This is described in eq. (8), T, F, C, b and a denotes the temperature, the laser fluence i.e. the energy per unit area, the heat capacity, the thickness of the graphite film and a free fit factor respectively [1]. The free fit factor is used to match the calculated and experimentally determined temperatures. The subscripts 1 and 2 denote whether it is the property of graphite or nickel respectively.

$$T(t = 0) = \begin{cases} \frac{aF}{\delta_1 C_1} exp(-z/\delta_1), & \text{for the graphite film: } 0 \leq z \leq b \\ \frac{aF}{\delta_2 C_2} exp(-b/\delta_1) exp(-(z-b)/\delta_2), & \text{for the nickel substrate: } b \leq z \end{cases}$$

$$(8)$$

The initial heat profile from the pump laser was calculated as described in eq. (8). The initial heat distribution can be seen in fig. 2a.

Using the expression in eq. (7) with the spacial and temporal boundary conditions described in section 1.3.2 and section 1.3.3 respectively the temperatures were updated by solving for $\mathbf{T}^{n+1}$. The temperature for all points in the graphite film was averaged and plotted against the respective time delay in order to give one curve. The modeled temperature curve was converted to strain using eq. (1) by multiplying the temperature difference with the thermal expansion coefficient of graphite. The strain in the graphite over time can be seen in fig. 2b.

2 Method

2.1 Principle of the experiment

The experiment was conducted at the FemtoMAX beamline at the MAX IV facility.

2.1.1 FemtoMAX setup

The FemtoMAX beamline is supplied with 3 GeV electrons directly from the linear accelerator (LINAC). The LINAC uses radio frequency cavities which are synchronized to accelerate the electrons as they pass through them. The LINAC is a stable source of accelerated electron bunches. The accelerated electrons travel in vacuum tubes to avoid collisions with molecules. [5]

Photons are created when electrical charges are accelerated. This is utilized to create the X-rays used in the FemtoMAX experiments from the 3 GeV electrons by using undulators. A undulator is constructed of many dipole magnets in alternating directions. This creates a magnetic field which accelerates the electrons back and forth in the transverse direction, which creates photons. In the FemtoMAX beamline there are two undulators, which can create X-ray pulses in the energy range of 1.85-20 keV and a pulse length of around 100 fs. Using a dipole dump magnet the electrons are directed away from the target and into a beam stop to ensure that they do not interfere with the experiments as well as to reduce the generated radiation for safety reasons. [5]
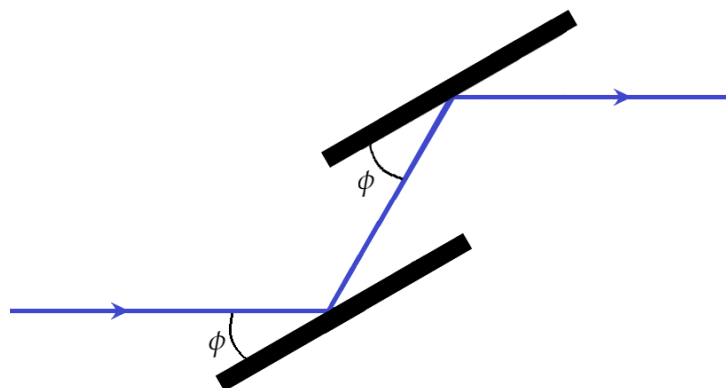

Figure 4: Illustration of a monochromator where ϕ is the Bragg angle.

The undulators create photons in a energy range which is a few percent of the selected energy. To select the desired wavelength a monochromator is used. An illustration of a monochromator can be seen in fig. 4. In a monochromator the incoming radiation (blue) is diffracted on crystal plates. The pulse is only correctly directed towards the sample if it has the correct Bragg angle (ϕ in fig. 4) and therefore as seen in eq. (4) the correct wavelength. The angle and distance between the plates can be varied to select which wavelength is directed towards the sample. Focusing mirrors are utilized to focus the radiation onto the sample. [5]

The pump pulse is created by an ultrafast laser system. The laser pulse is generated in a laser laboratory above the beamline, sent through the floor and directed into the
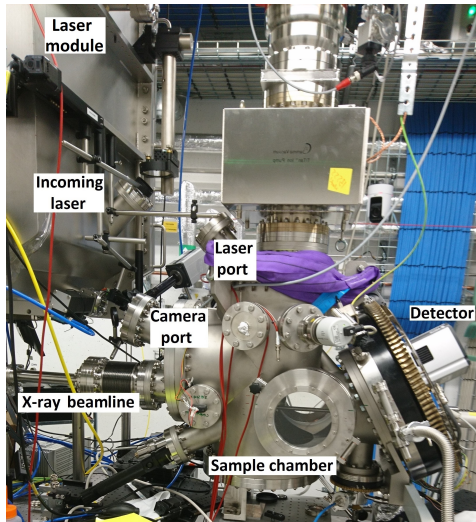
(a) Picture of the experimental setup with labels detailing objects of interest.
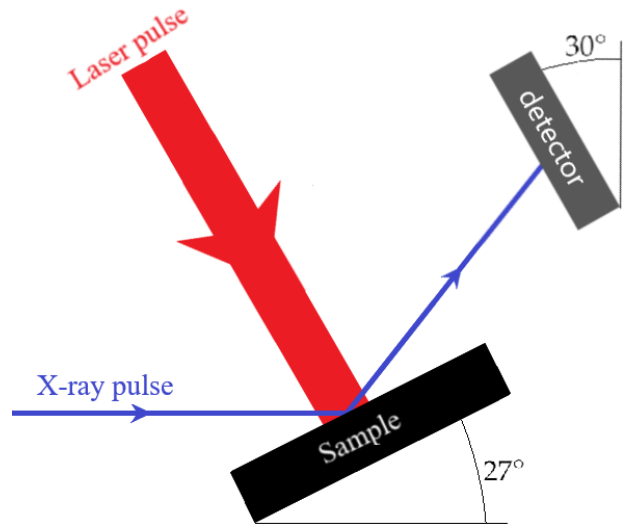
(b) Illustration of the setup inside the sample chamber with visualized laser and X-ray pulses. (Not to scale).

Figure 5: Illustrations of the setup.

sample chamber. fig. 5a shows the sample chamber, the laser module, the X-ray beamline and the detector. An illustration of the setup inside the chamber with visualized X-ray and laser pulses impinging on the sample can be seen in fig. 5b. The detector was rotated 30° from the vertical plane and the sample was rotated 27° from to the horizontal plane and incoming X-ray pulse as illustrated in fig. 5b. During the experiments the X-ray beam had a 2 Hz repetition rate. The repetition rate of the laser was matched with this. The pulse duration of the laser was 50 fs. [5]

A camera views the sample through a 30° titled camera port in fig. 5a, an image of the sample from this camera can be seen in fig. 6.
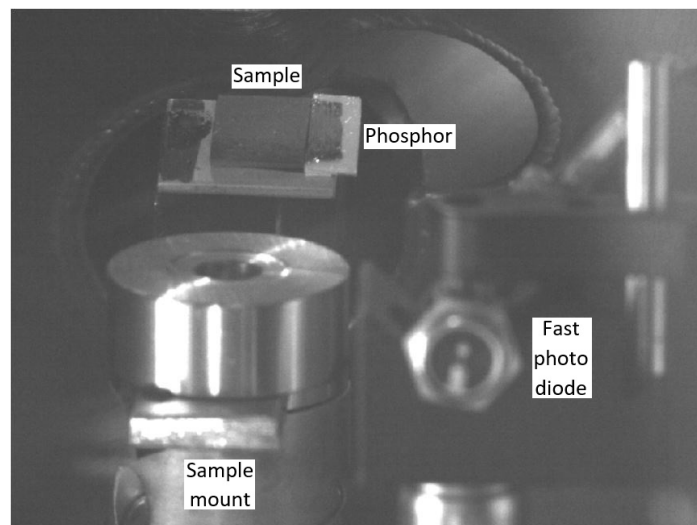

Figure 6: Picture of the sample in the sample chamber taken by the camera through the camera port.

The delay between these pulses is measured by the beam arrival monitor (BAM). The delay is calculated by taking two signals, one from the laser and one from the X-rays. Part of the laser is split of from the beam and sent into a laser diode to create the first signal. The other signal comes from a beam position monitor (BPM) which is triggered by the electron bunches. The BPM is located after the undulators. Because of the relativistic velocities, the Coulomb field of the electrons extends orthogonally to the direction of its movement. The BPM detects this field as the beam passes. The delay between these signals can not be determined directly as the oscilloscope sample rate is not fast enough to measure it accurately. Instead these two signals are sent through a band pass filter which creates two ringing signals. These signals are sampled and cross correlated, which creates a additional ringing signal. The phase of this signal provides information about the time delay. [6]

The X-rays are diffracted off the sample onto a window-less CCD detector where they are detected as intensity against pixel position creating an image (a two dimensional array with intensities) [5]. The detector was rotated slightly so that the diffraction images were recorded at an angle. The distance between the pixels is known. The measured data is thus recorded in the form of images of diffraction patterns with a corresponding BAM delay value.

2.1.2 Conducting the experiment
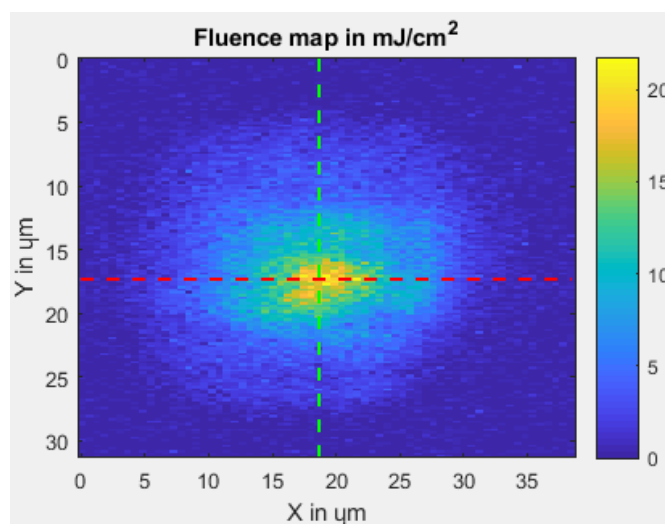
Figure 7: Laser profile.

In order to measure the laser fluence, the laser was directed onto the phosphor situated next to the sample (see fig. 6). The resultant fluorescent light was measured using the camera which is viewing through the camera port in fig. 5a. This results in the laser profile in fig. 7. The fluence was calculated as incoming laser energy which was known divided by the area of the spot which was measured using the camera.

The experiments were conducted utilizing the "pump-probe" method. This technique is comprised of first exciting the system using a pump pulse to cause a dynamic reaction. This reaction is investigated by using a probe pulse which documents the dynamical response [7]. In this experiment the pump pulse was a laser pulse which thermally

excited the sample and the probe pulse was the X-ray pulse which was diffracted onto the sample. The sample was mosaic meaning that it can reflect at all angles but only the angles which fulfill the Bragg condition gives rise to a diffraction spot. The sample was positioned so that a Bragg peak was created on the detector when the system was in equilibrium. As the system was excited by the laser pulse the Bragg angle shifted as described in the theory. This shift in the Bragg angle shifted the Bragg peak and through it the diffraction pattern. The time delay between these two pulses was scanned and from this a sequence of diffraction patterns were measured.

An illustration of the pump-probe method used can be seen in fig. 8, τ, θ and θ_0 are the time delay between pump and probe pulse (a positive time delay means that the pump pulse arrives before the probe pulse), the Bragg angle and the unexcited Bragg angle respectively.
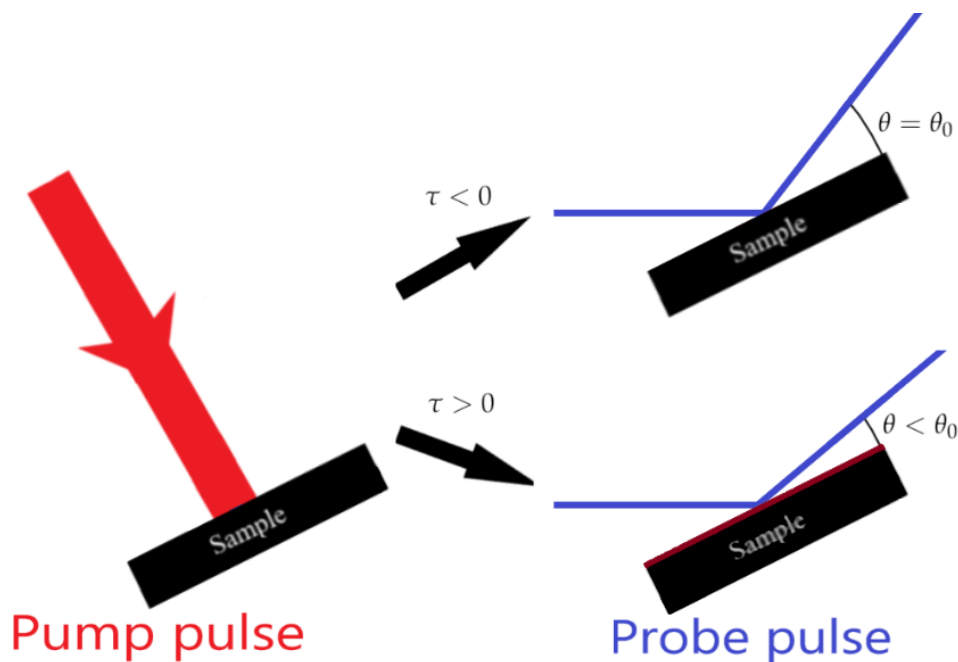
Figure 8: Illustration of the pump probe method

These measurements were done for three samples named the "10 minute", the "20 minute" and the "ESRF" sample. The ESRF sample is the same sample used in [1]. The minutes refer to the amount of time the graphite was deposited onto the nickel substrate. Each sample measurement was done for three different laser fluences. The same sample and fluence was measured several times to collect more data in order to reduce the statistical variation.

2.2 Analysis

2.2.1 Compiling the measured data

As mentioned in section 2.1.1 the measured diffraction patterns came in the form of images. Since the detection screen was rotated slightly, so was the diffraction patterns. To compensate for this, the rotated angle was estimated and the image was rotated

back. The background noise was removed by defining an intensity threshold and setting all pixel intensities under said threshold to zero. As the expansion of the material should only shift the diffraction pattern along one dimension the rotation limited the diffraction pattern to shift vertically. The center of gravity of each of the diffraction images was calculated. In fig. 9 two of these diffraction patterns are compared. The pattern to the left corresponds to a negative time delay and therefore a unexpanded sample, the pattern to the right corresponds to a positive time delay. Note that the center of the pattern, denoted by the black cross, has shifted as predicted in the theory, i.e. a larger interplanar distance results in a smaller Bragg angle.
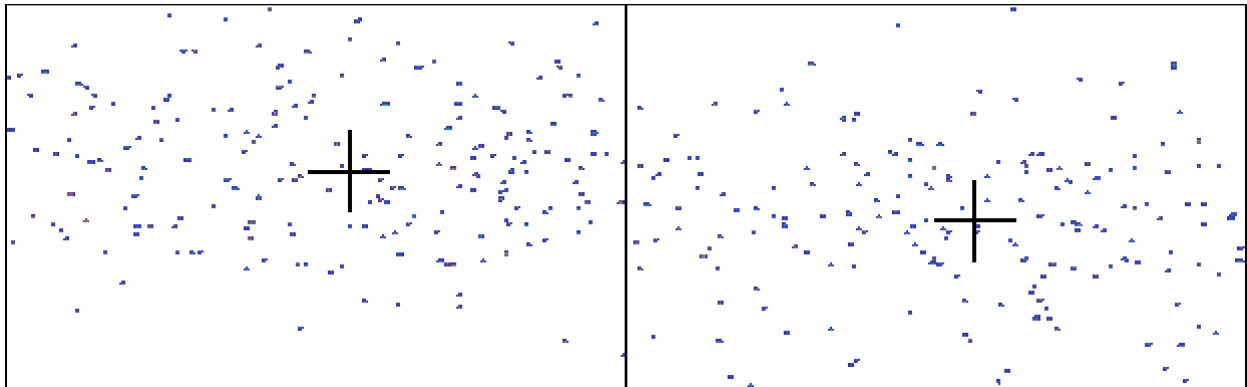

Figure 9: comparison of two diffraction patterns measured for negative time delay (left) and positive time delay (right). The black cross denotes the center of the diffraction patterns.

The vertical component of the center of gravity was plotted as a function of time delay between the two pulses. To limit the statistical variations, several measurements were combined. The time delays were divided into bins and all position values in a bin were averaged and plotted against the corresponding bin delay.

The time delay was shifted so that time zero was defined as just before the rise in position caused by the excitation of the laser. The position was shifted to be zero for negative time delays by offsetting the data by the average value of the positions for the negative times. Since it is the relaxation of the system which is of interest all values before zero were removed.

2.2.2 Converting to strain

To convert the measured data to strain, the setup must be considered. It can be seen in fig. 10. The position of the sample and detector corresponds to those in section 2.1.1. The incident angle of the X-rays with respect to the sample surface was 27°, which full-fills the Bragg condition when the material is unexpanded. This is defined in eq. (9) where θ is the reflection angle and the subscript 0 denotes that it concerns the unexpanded material.

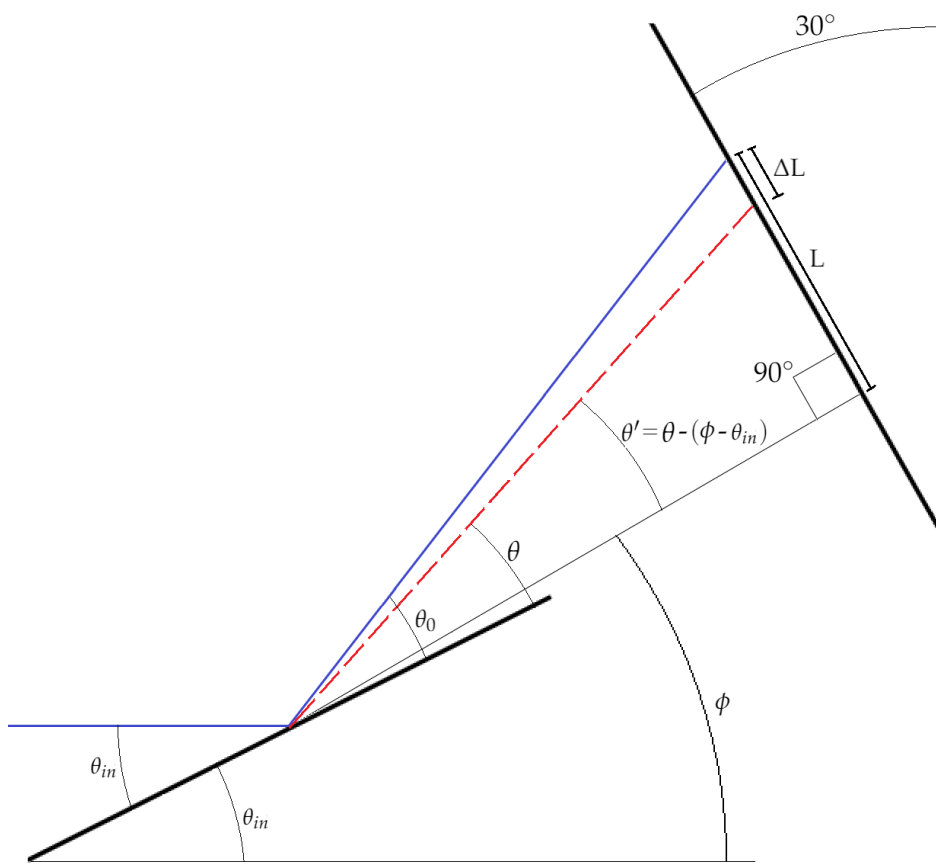$$\theta_0 = \theta(\Delta T = 0) = \theta_{in} \tag{9}$$

10

Figure 10: Illustration of the X-ray beam being reflected off of the sample and impinging on the detector. The Reflection off the unexcited material (blue full line) is compared to the reflection of the excited material (red broken line).

An expression for the strain can be obtained by reformulating eq. (4) and using the relation $d = d_0(1 + S)$ as illustrated in eq. (10) in which κ is a combination of constants.

$$\sin(\theta) = \frac{n\lambda}{2d} = \frac{\kappa}{d} \quad \Rightarrow \quad \frac{\sin(\theta_0)}{\sin(\theta)} = \frac{\kappa}{d_0} \frac{d}{\kappa} = \frac{d}{d_0} \quad \Rightarrow \quad S = \frac{\sin(\theta_0)}{\sin(\theta)} - 1 \quad (10)$$

Introducing the new angle θ' seen in fig. 10, where ϕ is the angle of the detector.

$$\theta' = \theta - (\phi - \theta_{in}) \quad (11)$$

The position on the detector is described in eq. (12) where l, D, L and ΔL is the position, the distance from the detector, the original diffraction position and the position shift described in fig. 10 respectively. Note that ΔL is the quantity which is measured in the experiment.

$$l = D\sin(\theta') = L - \Delta L = D\sin(\theta'_0) - \Delta L \quad (12)$$

The Bragg angle resulting from the of the excited sample is then described as seen in eq. (13).

$$\theta' = \arcsin\left(\frac{l}{D}\right) = \arcsin\left(\frac{D\sin(\theta_0) - \Delta L}{D}\right) = \arcsin\left(\sin\theta_0 - \frac{\Delta L}{D}\right) \quad (13)$$

Combining eq. (13) with eq. (10) and going back to the original angle using eq. (11) the conversion from position to strain (in fraction) is achieved using eq. (14).

$$S = \frac{\sin(\theta_0)}{\sin\left(\arcsin\left(\sin(\theta_0) - \frac{\Delta L}{D}\right) + (\phi - \theta_{in})\right)} - 1 \tag{14}$$

Hence, the position (ΔL) was converted to strain (S). By multiplying the right hand side of eq. (14) with 100 the strain in percent is derived.

An example of the resultant data from the compiling and converting is seen in fig. 11.
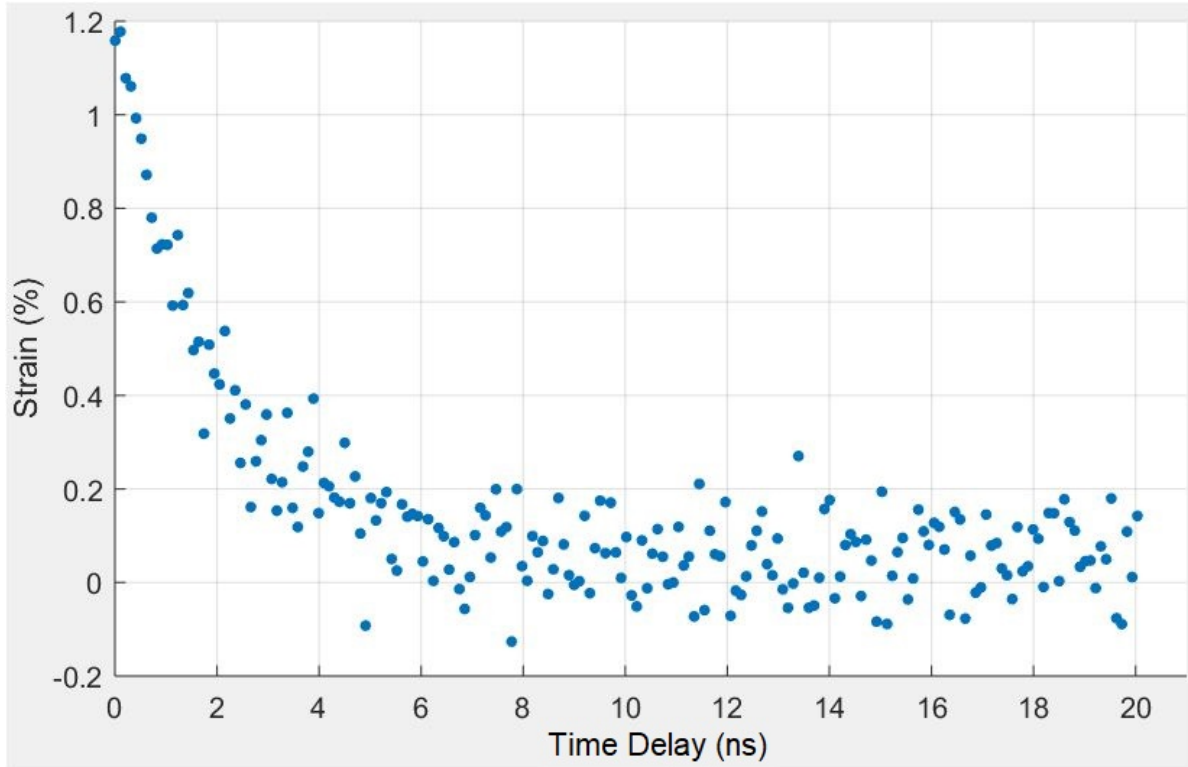
Figure 11: Plot showing an example of the compiled data from the experiment.

2.2.3 Estimating the thickness of the graphite films

The thicknesses of the graphite films of the different samples, needed in the modeling of the system, were unknown. This was calculated using eq. (3) by determining the expansion time of the sample as illustrated in fig. 12 where the difference in x value between the two points is the expansion time t_{exp}. The mean thickness of the different graphite films are documented in table 1. These were the thicknesses used in the fitting of the model to the measured values.

Table 1: Mean thickness of the different graphite films for different fluences.

Sample	Graphite thickness (nm)
ESRF	28
10 minutes	30
20 minutes	36

12
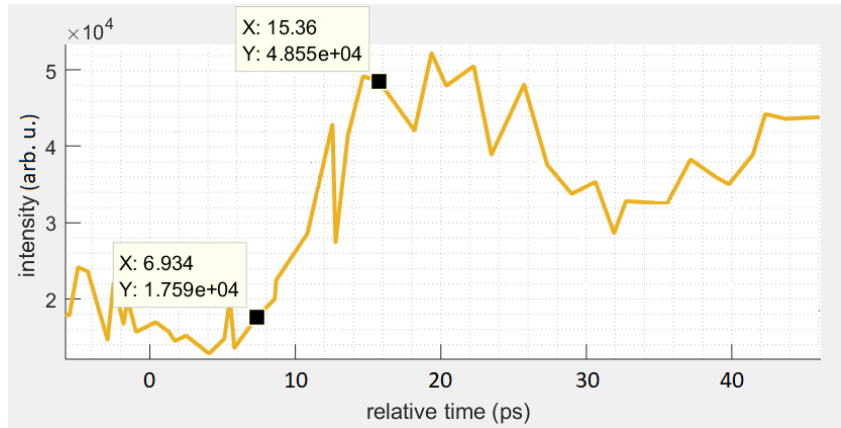
Figure 12: Illustrates the determination of the rise time for the 10 minutes sample at the 20 mJ(cm)$^{-2}$ fluence.

2.2.4 Fitting data to model
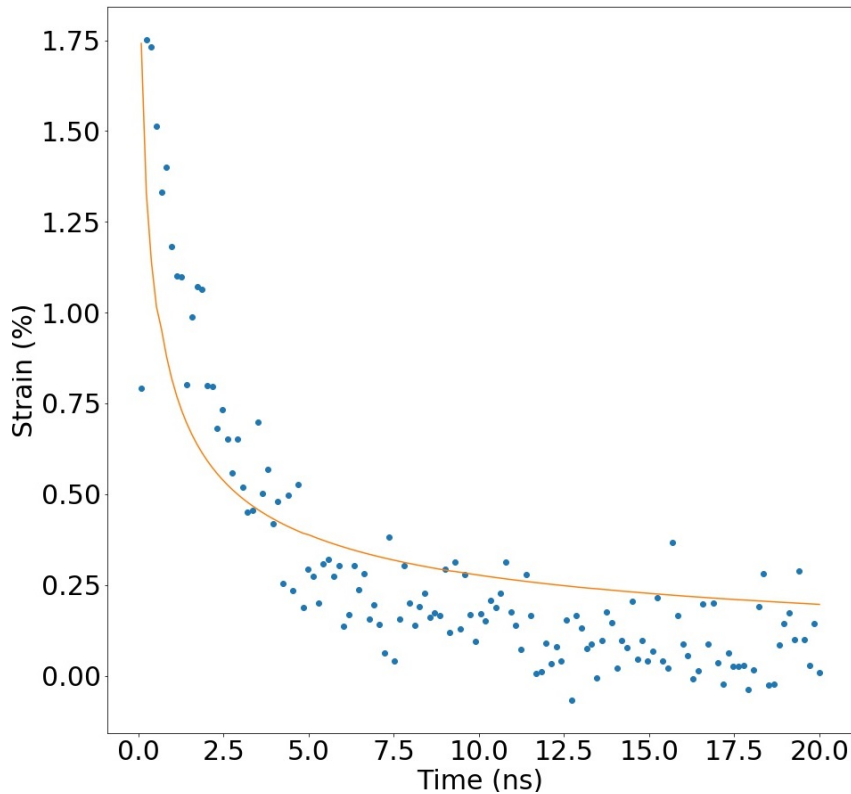
Figure 13: The fitted data of the ESRF sample for the fluence of 30 mJ(cm)^{2}. Shows measured data (blue dots) and fitted curve (yellow line) as strain against time.

The modeled strain curve (see fig. 2b) was fitted to the converted measured curve (see fig. 11). The thermal conductivity was determined by modeling it as a fitting parameter. The amplitude fit factor (seen in eq. (8) was also utilized in order to account for effects such as laser reflection off of the the sample resulting in less deposited laser energy. The temperature model fitted to the data can be seen in fig. 13. The parameter values used in the modeling can be seen in table 2.

13

The step sizes were increased after a number of steps to decrease the computational times without affecting the results. For the first time steps the differences in temperature between adjacent positions in the graphite nickel interface is large as can be seen in fig. 2a. After a number of time steps the heat distribution has smoothed out allowing for larger time steps to be used. This was also implemented in the space steps utilizing small steps from the graphite surface and well into the nickel and then successively increasing the space step size. The smallest step sizes were 1 nm in space and 0.1 ps in time.

Table 2: Parameter values used in the modeling.

Material	Parameter	Value	Source
Graphite	Volumetric heat capacity	$1.42 \cdot 10^6$ JK^{-1}m^{-3}	[9]
Graphite	Optical absorbation depth	140 nm	[10]
Graphite	Thicknesses	see table 1	Estimated see section 2.2.3
Graphite	Thermal expansion coefficient	$2.7 \cdot 10^{-5}$ K^{-1}	[11]
Graphite	Speed of sound	4140 ms^{-1}	[12]
Nickel	Volumetric heat capacity	$3.96 \cdot 10^6$ JK^{-1}m^{-3}	[9]
Nickel	Thermal conductivity	91 Wm^{-1}K^{-1}	[9]
Nickel	Optical absorbation depth	15 nm	[13]
	Fluence	200 and 300 Jm^{-2}	Measured
	Bragg angle	27°	Measured
	Detector angle	30°	Estimated
	Sample detector distance	0.15 m	Estimated

3 Results and discussion

To illustrate the results, the arrived at values for two fluences 20 and 30 $mJ(cm)^{-2}$ is presented for each sample. Four different results are presented, which differ in the assumptions made in the modeling. For each result thermal conductivity k depending on sample, fluence F and graphite film thickness b are presented. The fitted data for result A is presented in fig. 13 and for results B and C it is presented in Appendix B.

3.1 Result A

These results, presented in table 3, were obtained as described in section 2 using the values presented in table 2.

Table 3: Calculated values of the thermal conductivity of the graphite flakes depending on sample and fluences for the assumptions presented in section 2

Sample	F (mJ(cm)$^{-2}$)	b (nm)	k (Wm^{-1}K^{-1})
ESRF	20	28	18
10 minutes	20	30	24
20 minutes	20	36	37
ESRF	30	28	13
10 minutes	30	30	19
20 minutes	30	36	28

The attained results can be compared to the results determined in previous investigations of how the thermal conductivity depends on the thickness of the graphite films in [1, 15]. These results are presented in as thermal conductivity against film thickness in fig. 14.
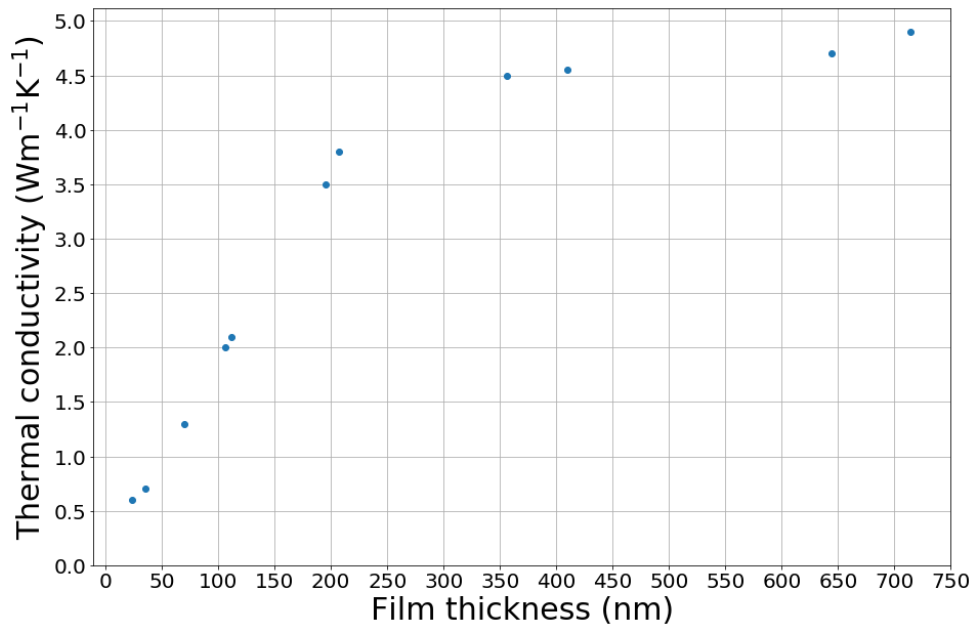

Figure 14: Results of thermal conductivity against film thickness from [15].

It is clear that the results in this work divert heavily from the values arrived at in [1, 15] as the thermal conductivity values are significantly larger than the values in fig. 14.

The thermal conductivity relations between the different samples seem to be in line with [15] since the thermal conductivity is increasing with the thickness of the film. From the results a connection between film thickness and thermal conductivity can be observed.

A trend that can be seen is that the data measured for higher laser fluences result in lower thermal conductivity. This shows a connection between deposited energy and thermal conductivity.

3.2   Result B

These results, presented in table 4, differ from Result A in that the thickness of all films were modeled as 80 nm in order to see how the modeled thickness affects the results. This is the thickness found for the 10 minute sample with ion beam milling [14].

Table 4: Calculated values of the thermal conductivity of the graphite flakes depending on sample and fluences with the thickness of all films put to 80 nm.

Sample	F (mJ(cm)$^{-2}$)	b (nm)	k (Wm^{-1}K^{-1})
ESRF	20	80	54
10 minutes	20	80	64
20 minutes	20	80	78
ESRF	30	80	33
10 minutes	30	80	52
20 minutes	30	80	65

The assumption of thicker graphite films results in increased thermal conductivity.

A connection between thermal conductivity and film thickness is also seen in this result. This connection can therefore be seen to not only be an effect of the modeling as it is also true in the case where the thicknesses were set to the same value.

3.3   Result C

In these results, presented in table 5, the ESRF sample was modeled with a film thickness of 35 nm in order to be compared to [1] in which the same sample was used and the thickness of the film was determined to be 35 nm. In [1] a fluence of 25 (mJ(cm)$^{-2}$) was utilized, which resulted in a thermal conductivity of 0.7 Wm^{-1}K^{-1}.

Table 5: Calculated values of the thermal conductivity of the graphite flakes depending on sample and fluences for the ESRF sample with film thickness 35 nm.

Sample	F (mJ(cm)$^{-2}$)	b (nm)	k (Wm^{-1}K^{-1})
ESRF	20	35	24
ESRF	30	35	18

As seen in table 5 the obtained results unfortunately diverge heavily from the determined values in [1].

3.4 Error sources

It seems reasonable to assume that there is some software problems in the modeled system which affects the results. This is clear as the results of [1] could not be recreated even though the same sample was used. Also the calculated thermal conductivity was larger than that of bulk graphite which contradicts the results in both [1, 15]. If there would have been more time available this would have been investigated and the software problems would have been corrected.

Other error sources include uncertainty in the thickness of the films. It is uncertain if the method for approximating the thickness of the graphite films was accurate. As discussed the thickness of the 10 minutes sample was measured to be approximately 80 nm. The ESRF sample which was determined to be 35 nm thick in [1] was estimated to be around 30 nm using the method in section 2.2.3. This could mean that the estimations of the film thickness yields values that are too small. This does not however account for the discrepancies with [1, 15] as it has been shown through comparing results A and B that increasing the thickness in the model increases the thermal conductivity.

Other error sources include ambiguity in the rotation of the detector. The rotation of the detector was determined by rotating an overnight diffraction image (an image which contains all diffraction points from X-ray shots taken over night on an unexpanded sample) and determining at which angle the diffraction pattern was correctly aligned by eye. This can give a error in rotation angle of some degrees. Whilst this would have an impact on the data it should only result in a scaling effect and thus not affect the thermal conductivity.

The distances between the sample and the detector was estimated but not measured meaning the uncertainty in the value is large. This should however only affect the converting of the measured data to strain which only scales the values. Thus this should not affect the thermal conductivity and should be accounted for by the amplitude fit factor.

The optical absorption depth of graphite used was experimentally determined and not the tabled value which is smaller. This value was chosen as it was the same used in [1] in order to reproduce the results arrived at in that article. The system was also modeled using the tabled optical absorption depth and whilst the thermal conductivity was reduced slightly it was not enough to account for the discrepancies between the results and [1, 15].

4 Conclusion and outcome

In this thesis TRXD has been shown to be used to investigate the thermal properties of nanomaterials. Whilst the results disagree with previews results it has been shown that the thermal conductivity can be investigated and that it is reduced with the thickness of the film. A connection between fluence (and through it deposited energy) and thermal conductivity was also observed as higher fluence resulted in lower thermal conductivity.

In order for the results to give useful information additional modeling needs to be done, in order to determine the thermal properties with higher certainty. This work is a first step towards such modeling and through it hopefully the effect due to the thickness of the material, on the thermal properties can be better determined. This is important both for the understanding of how heat transfers in nanomaterials as well as for the many possible applications of nanoscale graphite.

References

[1] M. Harb et al. Appl. Phys. Lett. **101**, 233108 (2012)

[2] *X-ray Diffraction*, B. E. Warren (Addison-Wesley, Massachusetts, 1969).

[3] *Solid State Physics: An Introduction*, P. Hofmann (wiley-VCH, Weinheim, 2008).

[4] *Fundamentals of Photonics*, B. E. A. Saleh, and M. C. Teich (Wiley, New York, 1991).

[5] H. Enquist et al. J. Synchrotron Radiat. Volume 25 Part 2 March 2018 Pages 570-579

[6] A. L. Cavalieri et al. PRL **94**, 114801 (2005)

[7] M. J. Rosker, M. Dantus and A. H. Zewail, J. Chem. Phys. 89, 6113 (1988)

[8] *Basic Concepts in Computational Physics*, A. Stickler and E. Schachinger, (Springer, New York, 2013).

[9] *CRC Handbook of Chemistry and Physics*, 92nd ed., edited by William M. Haynes (CRC, Boca Raton, FL, 2011).

[10] A. Hu, M. Rybachuk, Q.-B. Lu, and W. W. Duley, Appl. Phys. Lett. 91, 131906 (2007).

[11] E. A. Kellett and B. P. Richards. J. Appl. Crystallogr. 4, 1 (1971).

[12] M. Mohr, J. Maultzsch, and C. Thomsen, Phys. Rev. B 75, 153408 (2007)

[13] *Handbook of Optical Constants of Solids*, edited by E. D. Palik (Academic, Boston, 1985).

[14] A. Jurgilaitis, private communication, Mar. 2019.

[15] Q. Fu et al. Appl. Phys. Lett. **106**, 031905 (2015).

Appendices

A   Code

Python code for modeling and fitting the heat equation.

```python
from scipy import*
from pylab import*
from numpy import*
import matplotlib.pyplot as plt
import timeit
import scipy.optimize as opt


Files = ['Spectra10min20mJ_ny.txt','Spectra10min30mJ_ny.txt',
         'Spectra20min20mJ_ny.txt' , 'Spectra20min30mJ_ny.txt',
         'SpectraESRF20mJ_nynyny.txt','SpectraESRF30mJ_nyny.txt']
Flist = [ 200 , 300 , 200 , 300 , 200 ,  300 ]
dlist = [ 30e-9 , 30e-9  ,  36e-9 , 36e-9 , 28e-9 , 28e-9 ]


for iii in range(len(Files)):

    #%% Loading the data, which is converted to strain
    data = np.genfromtxt(Files[iii])
    xdata = data[:, 0]
    ydata = data[:, 1]

    #%% Constants That I Define
    start = timeit.default_timer()
    # constants
    C = [1.535e6,3.96e6]                         #volumetric heat capacity
    delta = [140e-9,15e-9]                       #optical absorbation depth
    F = Flist[iii]                               #incident fluence
    Texp = 27e-6                                 #thermal expansion coefcient
    knickel = 91

    # fit parameters
    kgraphite = 1                               #thermal conductivity guess
    aa = 1                                      #free fit paramater
    offset = 0

    d = dlist[iii]                              #graphite film thickness

    #define z variable
    a = [10e-10 , 30e-10 , 60e-10]              #position step size
    zsteps = [int(40 * d / a[0]) ,  int((20* d) / a[1]),  int((0 * d) / a[2])]

    #define t variable
    h = [0.1e-12 , 50e-12]                      #time step
```

20

```
tsteps= [200 , int((xdata[-1]-200*h[0])/h[1])]

#%% Constats That I Calculate
InterfaceIndex = int(d / a[0])                        #graphite nickel interface index
z = concatenate((linspace(0, a[0] * zsteps[0], zsteps[0]) ,
    linspace(a[0] * (zsteps[0]+1),a[0]*(zsteps[0]+1)+a[1]*zsteps[1],zsteps[1]),
    linspace(a[0] * (zsteps[0]+1)+a[1] * (zsteps[1]+1),
    a[0]*(zsteps[0]+1)+ a[1]*(zsteps[1]+1)+a[2]*zsteps[2],zsteps[2])))
zz=len(z)
time = concatenate((linspace(0,h[0] * tsteps[0],tsteps[0]) ,
        linspace(h[0]*(tsteps[0]+1),h[0]*(tsteps[0]+1)+h[1]*tsteps[1],tsteps[1])))

p = [kgraphite, aa, offset]

#%% Defining functions

def T01(z, d, aa, F, delta, C ):   #function to calculate time zero temperature
    if z<=d:
        T0=aa*F/(delta[0]*C[0])*exp(-z/delta[0])
    else:
        T0=aa*F/(delta[1]*C[1])*exp(-d/delta[0] - z/delta[1] + d/delta[1])
    return T0

def CNdef(p,h,C,a,knickel,zz,InterfaceIndex,zsteps):
 r1 = (p[0]/C[0])*h/a[0]**2                          #Matrix coefficients
 r2 = (knickel/C[1])*h/a[0]**2
 r3 = (knickel/C[1])*h/a[1]**2
 r4 = (knickel/C[1])*h/a[2]**2
 A = np.zeros((zz,zz))
 B = np.zeros((zz,zz))
 for i in range(zz):                                #define matrices A (LHS), B (RHS)
  if i==0:
   A[i,:]=[2+1*r1 if j==0 else (-r1) if j==1 else 0 for j in range(zz)]
   B[i,:]=[2-1*r1 if j==0 else r1 if j==1 else 0 for j in range(zz)]
  elif i==zz:
   A[i,:]=[-r4 if j==zz-2 else 2+2*r4 if j==zz else 0 for j in range(zz)]
   B[i,:]=[r4 if j==zz-2 else 2-2*r4 if j==zz else 0 for j in range(zz)]
  elif i <= InterfaceIndex:
   A[i,:]=[-r1 if j==i-1 or j==i+1 else 2+2*r1 if j==i else 0 for j in range(zz)]
   B[i,:]=[r1 if j==i-1 or j==i+1 else 2-2*r1 if j==i else 0 for j in range(zz)]
  elif i <= zsteps[0] and i > InterfaceIndex:
   A[i,:]=[-r2 if j==i-1 or j==i+1 else 2+2*r2 if j==i else 0 for j in range(zz)]
   B[i,:]=[r2 if j==i-1 or j==i+1 else 2-2*r2 if j==i else 0 for j in range(zz)]
  elif i <= zsteps[0] + zsteps[1] and i > zsteps[0]:
   A[i,:]=[-r3 if j==i-1 or j==i+1 else 2+2*r3 if j==i else 0 for j in range(zz)]
   B[i,:]=[r3 if j==i-1 or j==i+1 else 2-2*r3 if j==i else 0 for j in range(zz)]
  else:
   A[i,:]=[-r4 if j==i-1 or j==i+1 else 2+2*r4 if j==i else 0 for j in range(zz)]
```

```python
        B[i,:]=[r4 if j==i-1 or j==i+1 else 2-2*r4 if j==i else 0 for j in range(zz)]
    return A , B , r1

def CN(p,h,C,a,knickel,zz,InterfaceIndex,zsteps,z,d,F,delta,time,tsteps):

    u = zeros(zz)
    for i in range(len(u)):
        u[i] = T01(z[i], d, p[1], F, delta, C )

    umean = zeros(len(time))
    for j in range(len(tsteps)):
        A , B , r1 = CNdef(p,h[j],C,a,knickel,zz,InterfaceIndex,zsteps)
        bb = B.dot(u)
        for i in range(tsteps[j]):
            umean[i+j*tsteps[0]] = mean(u[1: InterfaceIndex-3])
            u[:] = np.linalg.solve(A,bb)
            bb = B.dot(u)

    Strain = umean * Texp * 100
    InterestStrain = zeros(len(xdata))
    for i in range(len(xdata)):
        InterestStrain[i] = Strain[find_nearest(time, xdata[i])]
#           InterestStrain[i] += p[2]

    return InterestStrain


def find_nearest(array, value):
    array = np.asarray(array)
    idx = (np.abs(array - value)).argmin()
    return idx

def residuals(p):
    return ydata - CN(p,h,C,a,knickel,zz,InterfaceIndex,zsteps,z,d,F,
                      delta,time,tsteps)

CN(p,h,C,a,knickel,zz,InterfaceIndex,zsteps,z,d,F,delta,time,tsteps)

stop = timeit.default_timer()
print('time test code: ' , stop-start)

#%% fitting
popt, msg = opt.leastsq(residuals, p)
yfit = CN(popt,h,C,a,knickel,zz,InterfaceIndex,zsteps,z,d,F,delta,time,tsteps)

#%% Rescale X for ploting
Ptime = time*1e9
Pxdata = xdata*1e9
```

```python
#%% plotting
figure(6*iii,figsize=(15,15))
plot(Pxdata,ydata,'o', label='Data')
plot(Pxdata,yfit , label='Fit')
tick_params(axis='x', labelsize=30)
tick_params(axis='y', labelsize=30)
plt.ylabel("Strain (%)", fontsize=30)
plt.xlabel("Time (ns)", fontsize=30)
plt.grid(False)
filename = '111 Nya dirichlet final figurer' +  Files[iii]  + '.jpg';
plt.savefig(filename)
plt.legend()
plt.show()

stop = timeit.default_timer()
print('\nSpectra' , Files[iii] ,
      '\nThermal Conductivity' , popt[0] ,
      '\nAmplitude fit factor' , popt[1] ,
      '\nOffset' , popt[2] ,
      '\ntime whole code: ' , stop-start)
```
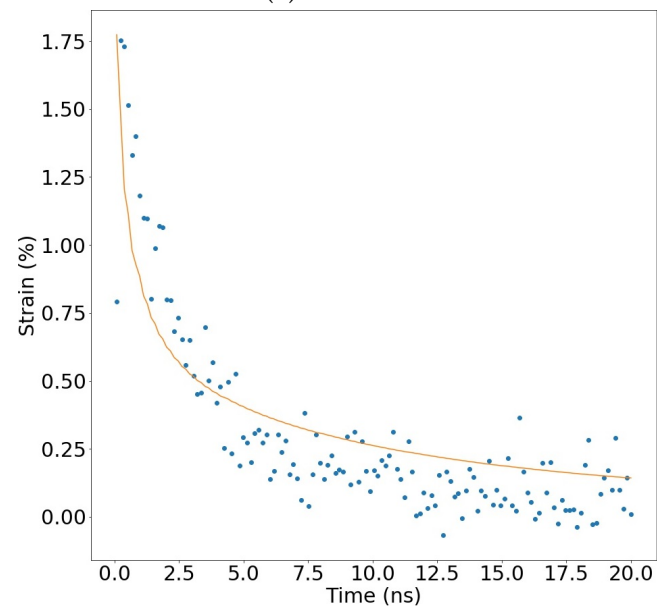
B Plots
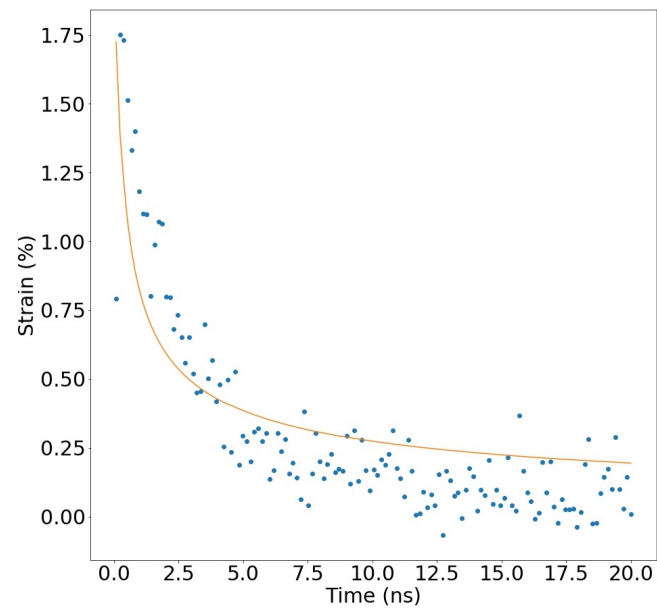
(a) Result B

(b) Result C

Figure 15: The fitted data of the ESRF sample data for the fluence of 30 $mJ(cm)^{-2}$. Shows measured data (blue dots) and fitted curve (yellow line) as strain against time for results B and C.